Numerical and experimental investigations of buffet on a diamond airfoil designed for space launcher applications

Jéromine Dumon, Yannick Bury and Nicolas Gourdain
DAEP, ISAE-SUPAERO, Toulouse, France, and

Laurent Michel
Institut Clement Ader (ICA), CNRS-INSA-Mines Albi-UPS, University of Toulouse, Toulouse, France and DMSM, ISAE-SUPAERO, Toulouse, France

Abstract

Purpose The development of reusable space launchers requires a comprehensive knowledge of transonic flow effects on the launcher structure, such as buffet. Indeed, the mechanical integrity of the launcher can be compromised by shock wave/boundary layer interactions, that induce lateral forces responsible for plunging and pitching moments.

Design/methodology/approach This paper aims to report numerical and experimental investigations on the aerodynamic and aeroelastic behavior of a diamond airfoil, designed for microsatellite dedicated launchers, with a particular interest for the fluid/structure interaction during buffeting. Experimental investigations based on Schlieren visualizations are conducted in a transonic wind tunnel and are then compared with numerical predictions based on unsteady Reynolds averaged Navier Stokes and large eddy simulation (LES) approaches. The effect of buffeting on the structure is finally studied by solving the equation of the dynamics.

Findings Buffeting is both experimentally and numerically revealed. Experiments highlight 3D oscillations of the shock wave in the manner of a wind flapping flag. LES computations identify a lambda shaped shock wave foot width oscillations, which noticeably impact aerodynamic loads. At last, the experiments highlight the chaotic behavior of the shock wave as it shifts from an oscillatory periodic to an erratic 3D flapping state. Fluid structure computations show that the aerodynamic response of the airfoil tends to damp the structural vibrations and to mitigate the effect of buffeting.

Originality/value While buffeting has been extensively studied for classical supercritical profiles, this study focuses on diamond airfoils. Moreover, a fluid structure computation has been conducted to point out the effect of buffeting.

Keywords Buffet, Wind tunnel test, URANS, LES, Fluid structure interaction, Composite

Paper type Research paper

This work is partially funded by the French Space Agency (CNES); this support is greatly acknowledged. The authors particularly thank Jean Oswald and FlorentPuel from DLA (Direction des LAnceurs) at CNES for their help on this study. The experimental campaign was conducted with the technical team of ISAE Supaero (special thanks to Emmanuel Rivet, Patrick Cheze and Marc Grellet). The simulations performed were achieved using CALMIP computing means, under project p1425 and GENCI A0042 A07178.

DOI 10.1108/HFF-07-2018-0353

Nomenclature

α	Angle of attack [rad];
α_0	Initial angle of attack [rad];
C	Chord of the aileron [m];
γ	Heat capacity ratio [ ];
D	Damping matrix;
E	Young's modulus [Pa];
F_A	Aerodynamic forces [N];
f_i	Frequency [Hz];
F_{lift} or F_Y	Lift force [N];
F_X	Drag force [N];
G	Shear modulus [Pa];
k	Stiffness of the solid [N/m or N.m];
K	Stiffness matrix [N/m];
L	Span of the aileron [m];
m	Mass of the solid [kg];
M	Matrix of mass [kg];
m^*	Mass ratio between the solid and the fluid [ ];
Ma	Mach number [ ];
P	Static pressure [Pa];
Pi	Stagnation pressure [Pa];
ρ	Local flow density [kg/m^3];
ρ_∞	Upstream flow density [kg/m^3];
S	Reference surface of the aileron [m^2];
St	Strouhal number [ ];
θ	Rotational displacement of the aileron [rad];
U_∞	Upstream flow velocity [m/s];
U^*	Normalized velocity based on ratio between the fluid velocity and the solid displacement velocity [ ];
v*	Maximum displacement velocity [ ];
x	Position vector of the solid [m/s];
x+, y+, z+	Dimensionless wall distance in axial, normal and span wise direction, respectively [ ];
y	Displacement of the aileronin the vertical direction [m]; and
y*	Normalized displacement [ ].

1. Introduction

Microsatellite-dedicated launchers, for which payload is lower than 50 kg, are of paramount importance for future space missions. Among the difficulties encountered for the design of such launchers, the aero-elastic behavior of the ailerons in transonic regimes still remains partly unknown. Such ailerons are originally designed to provide stability to the launcher, especially when lateral winds are experienced. The present work takes place in the frame of the PERSEUS' project (French acronym for Academic and Scientific European Student Project for Space Research) led by CNES, the French Space Agency, to promote the emergence of innovative technical solutions for space launchers. More precisely, this work focuses on the Supersonic Experimental Rocket ARES (SERA) series launchers (Figure 1).

To improve the stability of the rocket, SERA is equipped with three ailerons, composed of diamond airfoils made in a composite material. With the objective to increase their reliability in turbulent transonic flows, it is necessary to better understand the interactions between the unsteady flow, including shock induced flows, and the composite walls.

Moreover, such information is relevant in the context of reusable launchers, where the number of cycles that can be accomplished by the aileron must be accurately predicted.

It is thus necessary to predict the loads induced by the buffeting, to ensure that structure components and subsystems have adequate strength, stress and fatigue margins in regard to the structural dynamic response. Buffeting is a well-known instability, which occurs in the transonic regime. Buffet is characterized by fluctuating pressures resulting from flow-induced turbulence, flow separation, wake effects and shock oscillations. The interaction between the shock wave and the separated boundary layer causes the inception of instabilities responsible for a self-sustained periodic motion of the shock wave over the surface of the airfoil. In a typical flight of a SERA rocket, the transonic regime occurs during less than 2 s during its atmospheric phase as shown in Figure 2. These two seconds may, however, be decisive for the success or failure of the mission.

Transonic buffet is observed in many aeronautical applications, including internal flows (e.g. compressor) and external flows (e.g. aircraft wings). This phenomenon has been extensively studied in the past, and is still today, see for example the works of Pearcey and Rao (1968), Tijdeman (1968) and Lee (2001), thanks to experimental campaigns on reference geometries (McDevitt *et al.*, 1976; McDevitt and Okuno, 1985; Lee, 1990; Jacquin *et al.*, 2009; Sugioka *et al.*, 2015) or numerical simulations (Barakos and Drikakis, 2000; Renaud *et al.*, 2001; Brunet, 2003; Goncalves and Houdeville, 2004; Thiery and Coustols, 2006; Brunet and Deck, 2008; Iovnovich and Raveh, 2012; Sartor and Timme, 2016). Fundamental works have also been conducted, showing that global stability analysis is an accurate numerical tool to predict such unsteady flow phenomena (Iorio *et al.*, 2014; Sartor *et al.*, 2015). Analytical models have been developed to study the onset of buffeting, with a particular emphasis on control Burnham *et al.* (2001). Based on this extensive knowledge, it is possible to delay or alleviate buffeting in such geometries (Corre *et al.*, 2003; Caruana *et al.*, 2005 and Gao *et al.*, 2017). Unfortunately, the detailed mechanisms that are

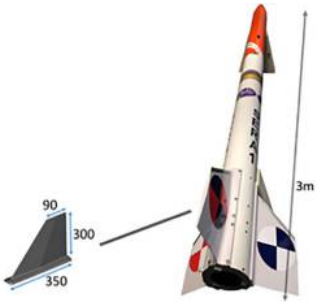

Figure 1.

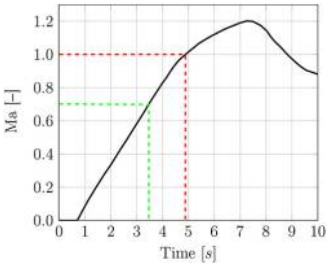

Figure 2.

responsible for the inception of the buffeting phenomenon and its dynamics are still nowadays debated (Crouch *et al.*, 2009). Moreover, contrary to classical supercritical profiles designed for civil aircrafts, there is a lack of studies for diamond airfoils, adapted to supersonic flows, which are the target of this work.

The first part of this paper deals with the experimental and numerical methods that have been used to study the inception of buffet in a diamond airfoil. In a second part, aerodynamic data are compared and analyzed, to highlight some of the mechanisms related to buffet for a non-moving airfoil. In the last part of the paper, numerical simulations are conducted, considering a moving airfoil, that dynamically responds to aerodynamic forces. Finally, some conclusions and perspectives are drawn.

2. Methods

2.1 Experimental setup

The ISAE-SUPAERO transonic wind tunnel has a 130 mm-by-80-mm rectangular test section. It is powered by four vacuum pumps and provides flow Mach numbers ranging from 0.7 ± 0.05 to 1.3 ± 0.1. Here, the Mach number is determined from the measurements of stagnation pressure Pi and static pressure P according to equation (1), with Ma the Mach number and γ the heat capacity ratio.

$$\frac{P}{P_i} = \left(1 + \frac{\gamma - 1}{2} Ma^2\right)^{\frac{\gamma}{\gamma - 1}} \tag{1}$$

Time-resolved Schlieren visualizations are recorded using a high speed Photron camera. Two sets of data can be recorded: 704 × 512 pixels' image with an acquisition frequency of 20,000 frames per second or a 512 × 272 pixels' image with an acquisition frequency of 50,000 frames per second. However, Schlieren technique intrinsically integrates 3D information into a 2D image. This makes difficult the analysis of the images when the flow naturally exhibits transient 3D structures and is then responsible for a hard-to-quantify inaccuracy in the shock wave spatio-temporal tracking, for instance.

The aileron dimensions are 80 mm in span and 50 mm in chord, with a symmetric diamond shape (Figure 3). Its thickness is set to 12 per cent of the chord, corresponding to a thickness of 6 mm. Such dimensions, with the Mach numbers considered in this work, correspond to a Reynolds number of about 700,000. The mock-up is fixed on one of the transparent glass window of the wind tunnel test section (Figure 4), on a rotating device

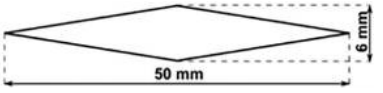

Figure 3.

Figure 4.

allowing to change the angle of attack of the aileron. The 0° angle is determined on the basis of the Schlieren images revealing the symmetric distribution of the shock waves on both sides of the WT model. The accuracy of the aerodynamic angle is estimated to 0.5° via post processing images of calibration targets. The angle of attack can be set from −2° to 2° by steps of 0.5°.

The boundary layer is not tripped in the wind tunnel. The laminar toturbulent transition naturally occurs after the crest, such that the buffeting phenomenon occurs in a region where the boundary layer is turbulent.

To determine the potential occurrence of a coupling between the characteristic frequencies of the flow (in particular with the oscillating shock waves) and a specific vibratory frequency of the aileron, a modal analysis is conducted on a vibrating pot (Figure 5). The setup of the aileron on the vibrating pot is chosen similar to its setup in the wind tunnel model (Figure 4), taking into account both the fixing beam of the aileron to the wind tunnel structure and the window in close contact with the aileron. The modal analysis reveals three main natural frequencies f_1 196 Hz, f_2 226 Hz and f_3 850 Hz. The frequency f_3 is associated with the fixation of the window to the vibrating pot, while f_1 and f_2 correspond to the two first flexion modes.

The predicted aerodynamics frequencies are away of the above-mentioned structural frequencies, which ensures that the potential occurrence of pressure fluctuations on the surface of the aileron due to the buffeting phenomenon and to other flow unsteadiness during the wind tunnel tests will not be induced or enhanced by the structural deformation of the aileron; and that the aileron will not experience severe deformation promoted by the aerodynamic excitation and its coupling with the structural deformation of the model under resonant effects.

On the basis of the time-resolved Schlieren visualizations, a spectral analysis of the shock wave oscillation is proposed, based on a three-step process:

(1) a one pixel-height sensor line is selected in the oscillation area (Figure 6 – left);

(2) a time series of the grey level signal is then extracted (Figure 6 – right); and

(3) the power spectral density of this signal can be computed (if the signal is periodic).

2.2 Numerical setup

The numerical analysis is performed with both unsteady Reynolds averaged Navier–Stokes (RANS) and large eddy simulation (LES) approaches, considering the operating conditions of the wind tunnel (including wind tunnel walls). Perturbations generated in the subsonic part of the boundary layer and in the wake of the aileron can travel upstream and impact the

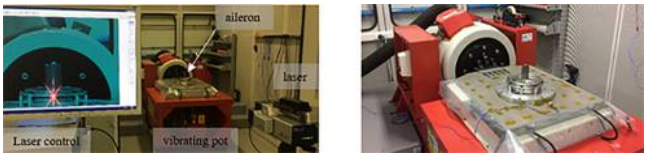

Figure 5.

Figure 6.

shock development in the zone of the lambda-shaped shock pedestal, so a particular care should be brought to the grid in the boundary layer region.

The numerical model used in the URANS approach is purely two dimensional, in order to reduce computational time effort, corresponding to the mid-section of the aileron (Figure 3). The dimensions of the computational domain are similar to those of the wind tunnel test section (130 mm high and 30 chords long).The center of the model is located 10 chords downstream from the inlet of the domain. For the LES computations, the 2D section of the actual wind tunnel model is extruded in the span-wise direction, with a span corresponding to 25 per cent of the chord, to ensure uncorrelated turbulence.

The URANS simulations are performed using STAR-CCM+ v11.02. The k-ω SST-Menter turbulence model (Menter, 1994) is used for turbulence modeling. A compressible solver is used with a second-order Runge–Kutta scheme for the time discretization. The spatial discretization of the convective fluxes is performed with a third-order MUSCL scheme. Regarding the grid, an unstructured polyhedral 2D mesh is used, based on prism layers close to the airfoil walls and polyhedral cells in the rest of the computational domain. The size of the mesh is highly refined close to the aileron surface, and in the zone where the shock waves are expected to develop. The prism layers are set on the aileron and wall surfaces to better capture the flow gradients inside the boundary layer. The size of the first layer was chosen to impose $y+<0.5$ on the aileron surfaces. A grid convergence study was performed, showing that a 1 million cell mesh is sufficient to ensure convergence on lift and drag coefficients while capturing the buffet phenomenon.

The numerical simulations are run in turbulent mode. However, based on the previous considerations about the state of the boundary layer in the wind tunnel, a numerical simulation with a transition model "Gamma-Re-Theta" has been performed to study the influence of transition on buffeting. The results show that the onset of buffeting and its frequency are not modified by the transition of the boundary layer. However, the magnitude of the shock displacement is reduced by about 30 per cent compared to the fully turbulent case. The main objective of the present work is to investigate the mechanisms related to the onset of buffeting and its interaction with the structure (and not the amplitude of the shock displacement). Thus, due to the computational overcost of the transition model, all URANS simulations reported in this paper are carried out in a fully turbulent mode.

LES computations are performed using the CharLESX solver (Bermejo-Moreno *et al.*, 2014), which solves the spatially filtered compressible Navier–Stokes equations with a finite volume formulation on unstructured hexahedral meshes. A fourth-order central scheme is used for the computation (second order on stretched volumes as in the present study). An explicit third-order Runge–Kutta (RK3) scheme is used for time integration with the Vremansubgrid-scale (SGS) model (Vreman, 2004). The approach relies on the combination of a non-dissipative centered numerical scheme and an essentially non-oscillatory (ENO) second-order shock-capturing scheme, with a shock sensor (Bermejo-Moreno *et al.*, 2014). Two grid strategies have been considered. The first one relies on a wall-modelling approach, with $y+\sim15$, $x+\sim30$ and $z+\sim50$, leading to a 30 million cells grid. The second method relies on a wall resolved approach (Kawai and Larsson, 2012), with $y+\sim1$, $x+\sim30$ and $z+\sim20$, that leads to a 120 million cells grid. Beyond the mesh size reduction, the main interest with the wall-modelling approach is the possibility to increase the time step by a factor of 10 in contrast to the wall resolved approach. Indeed, the cost ratio between wall resolved and wall modelling approaches is around 40.

As shown in Figure 7, for URANS computations, the inlet and outlet flow conditions are modelled as freestream and the walls are considered as adiabatic with a no-slip condition.

For LES computations, total pressure and temperature are imposed at the inlet, static pressure at the outlet and walls are considered as adiabatic with a no-slip condition.

3. Analysis of results

Shock wave and separated boundary layer oscillations are observed in both experiments and numerical simulations (Figure 8). A 3D flow visualization of the wall-resolved LES calculation shows the various scales of the resolved turbulence (Figure 9).

On the basis of URANS computations, buffeting is numerically found to occur for Mach numbers ranging from Ma 0.73 to Ma 0.81.Wind tunnel experiments did not permit to confirm these predictions because of technical limitations of the wind tunnel. Indeed, measurements did not give access to the inception of the transonic regime. It is thus not possible to experimentally determine the lower Mach value for the occurrence of buffeting.

The analysis of the Schlieren-based data shows an aperiodic three-dimensional, time-varying deformation of the shock wave in the span-wise direction (Figure 10).

A secondary oscillation of the shock wave is observed in both numerical and experimental data: the local boundary layer separation induces an oblique weak shock wave in front of the strong shock wave, resulting in a classical delta shaped pedestal. While the

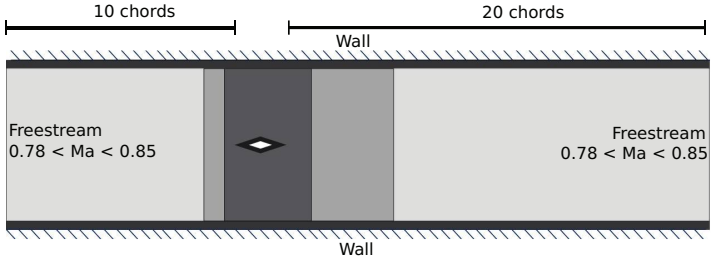

Figure 7.

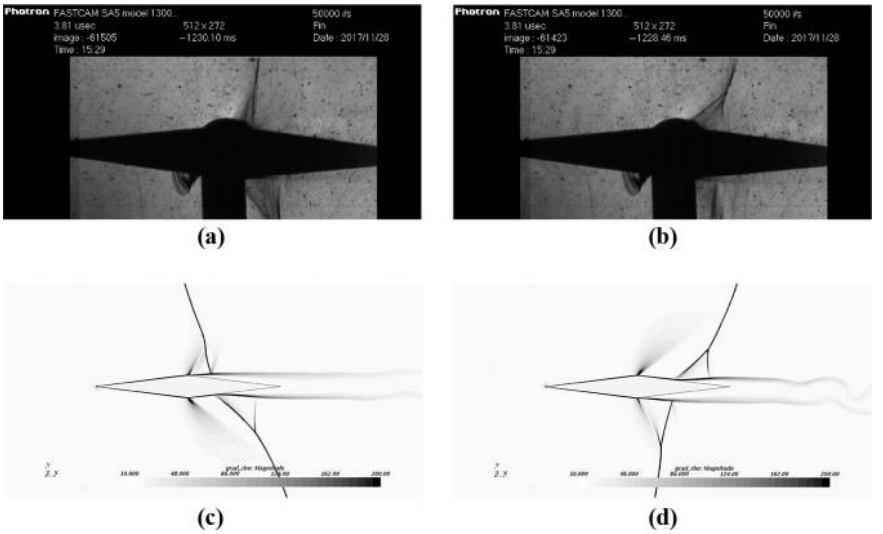

Figure 8.

dominant frequency results from the interaction between the strong shock wave and the boundary layer separation, the secondary oblique shock wave also oscillates due to the local periodic flow separation in front of the strong shock wave.

While URANS data exhibit strictly periodic trend of the flow, experimental data exhibit a chaotic behavior. Two states can be distinguished in this chaos: the "delta state" and the "flag state" (Figure 11). The delta state (Figure 11 upper right) corresponds to the sinusoidal oscillation of the shock wave. To be more precise, both the oblique weak shock wave and the strong shock wave oscillate at the same frequency. For this state, the flow can reasonably be considered as two dimensional. The flag state (Figure 11 down right) corresponds to a flow regime where the shock wave deforms in the span-wise direction, in the manner of a wind-flapping flag. At this stage of the study, the detailed analysis of this specific unstable state is still limited by the lack of experimental data. In particular, due to the 2 D spatial integration of the Schlieren technique, it cannot be confirmed if it is or not periodic. When the shock wave is experiencing the delta state, it is positioned closer to the trailing edge than when it is experiencing the flag state (Figure 11 left). Finally, a third state, hereafter denoted "flying state" can also be transiently observed as the shock wave tends to travel, but fails to, from the "delta state" to the "flag state" mean positions. Figure 12 depicts the temporal evolution of the shock wave states and of their transitions from the flag state – number 1 in the figure – to the delta state – number 4 in the figure – and reversely, and the transient occurrence of the "flying state" – number 3 in the figure.

With an angle of attack equal to 2°, both flag and delta states are present. But contrary to the previously discussed 0° angle of attack, the scenario does not alternatively switch from one state to the other state. The flag state is present on the suction side of the aileron and the delta state on the pressure side. This tends to indicate that the adverse pressure gradient may fuel the flag state.

The frequency of the shock wave oscillation is evaluated to f 620 Hz (URANS) and f 310 Hz (LES) with the spectral analysis. However, the results should be considered with

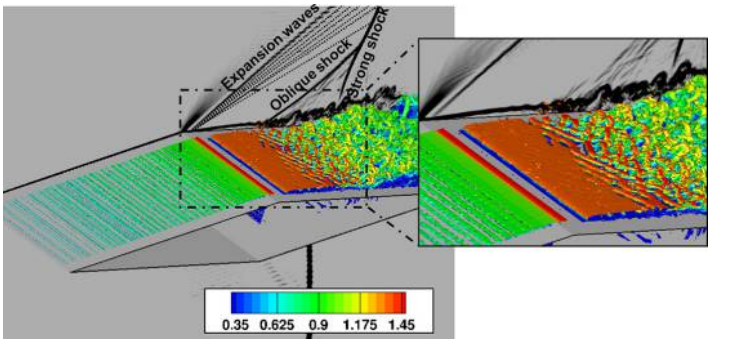

Figure 9.

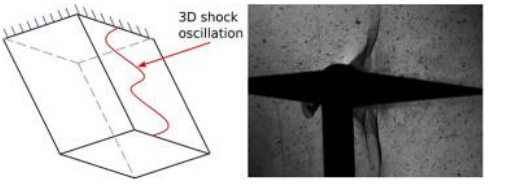

Figure 10.

caution for LES due to the limited amount of time available. As mentioned, the analysis of the Schlieren-based data remains difficult due to the presence of the three-dimensional nature of the shock wave.

The delta state is a periodic regime, as revealed by the extraction of the shock wave displacement as a function of time on the Schlieren images (Figure 12). An oscillating frequency of 4.7kHz is determined for the delta state.

Figure 13(a) and (b) depicts the standard deviation of the density fields based on both LES and URANS computations. Figure 13(c) shows cumulated density gradient fields based on time resolved Schlieren images obtained in the wind tunnel. These two complementary post-processing approaches provide similar information on the displacement amplitude of the shock wave during buffeting.

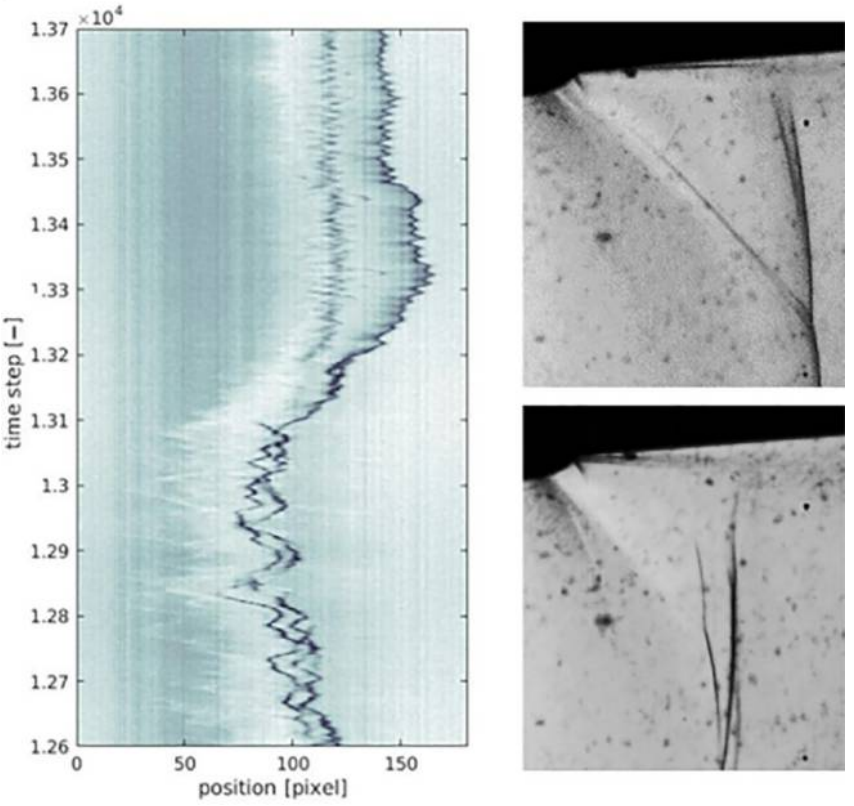

Figure 11.

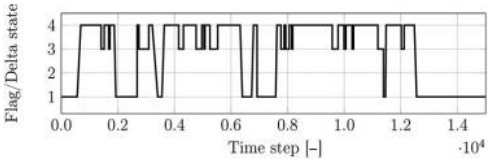

Figure 12.

The magnitude of the shock wave oscillations varies depending on the method used (LES, URANS or measurement). It is worth to mention that the angle of attack in the experimental setup is not strictly equal to 0°, as revealed by a non-strictly symmetric distribution of the shock wave footprint. Relatively to the wind tunnel results, the amplitude of the shock wave oscillations is better predicted with LES than with URANS. However, the mean position of the shock wave is better predicted with URANS than with LES. These could be caused by the potential influence of the boundary layer development on the lateral walls on the shock wave position, for a given Mach number. This is however difficult to predict.

The aerodynamic loads are unsteady due to the shock wave oscillations, as shown in Figure 14. Indeed, the lift and drag oscillations are driven by the buffeting phenomenon. The fast fourier transform (FFT) shown in Figure 14 highlights a frequency peak at 516 Hz and its harmonics. The Strouhal number, based on the upstream velocity and the chord, is equal to 0.089.

The analysis of load signals is not straightforward. Interestingly enough, correlations between instantaneous flow fields and lift temporal signals reveal that the instant for which the lift is null does not correspond to the instant when the shock waves are symmetric on

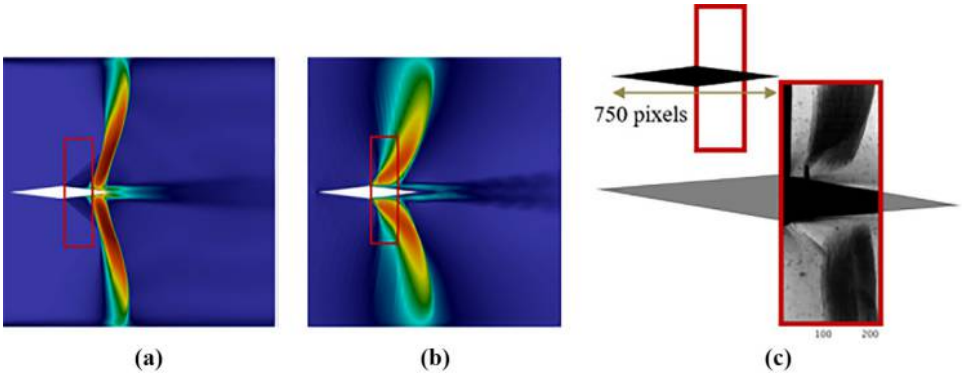

Figure 13.

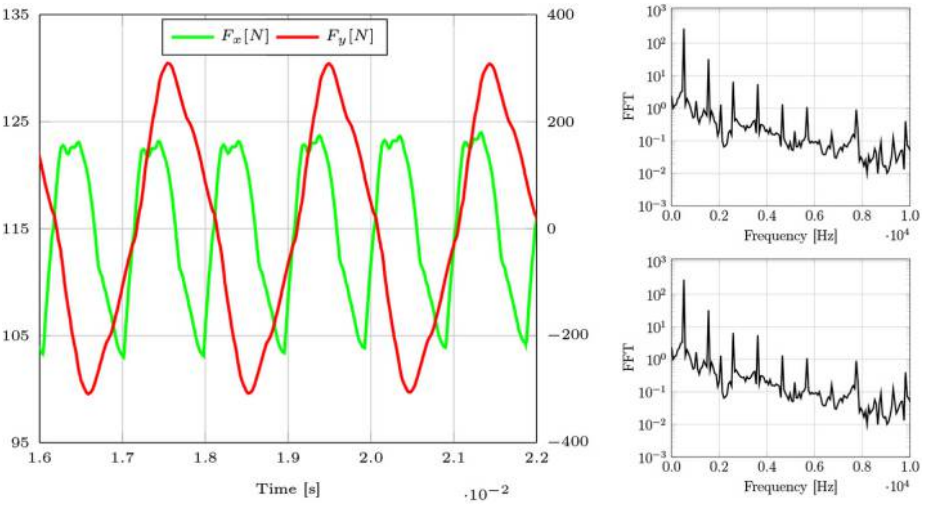

Figure 14.

both sides of the airfoil. This behavior is explained by the dynamics of the shock wave, which is different depending on its direction of displacement (upstream or downstream). This shock wave dynamic is thus associated with both lift and drag signals which are not sinusoidal, which in turn explains why the zero lift is not achieved when the positions of the shock waves are symmetric. This analysis also shows that the drag frequency is twice the lift frequency.

The lift and drag predicted with the wall-resolved LES are shown in Figure 15. Only one period of the shock wave oscillation has been simulated at the moment, which is insufficient to fully analyze the spectral content of the signal. However, these results highlight two main frequencies: one low frequency associated with buffeting and one higher frequency, related to the oblique shock wave oscillation. The magnitude order in terms of lift and drag are similar to URANS predictions.

4. Fluid structure interaction: impact of buffeting on the aileron

The objective here is now to study the effect of aerodynamic forces on the dynamic response of the profile. As a first approximation, only rigid movements of the aileron are considered, such as bending and torsion, as shown in Figure 16(a). The 3D aileron is reduced to its 2D extruded shape. The bending is modeled by a pure vertical translation in the plane while the torsion is modeled by a rotation in the plane, as in in Figure 16(b).

The aileron on the rocket is made of a sandwich composite material. The core is an epoxy foam and the skin is a carbon laminate. The aileron is considered as a beam with a thin web cross section. Moments of inertia are then calculated geometrically, for a diamond cross section of diagonals equal to 220 mm and 12.5 mm, with a 1 mm [...] thick web [...] corresponding to the laminate skin. The Young's modulus E and the shear modulus G are material properties, determined by the Classical Laminate Theory (Berthelot, 2012). The stiffness results are presented in Table I.

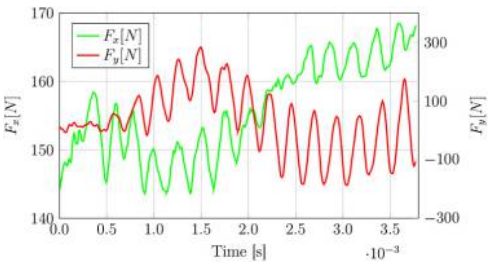

Figure 15.

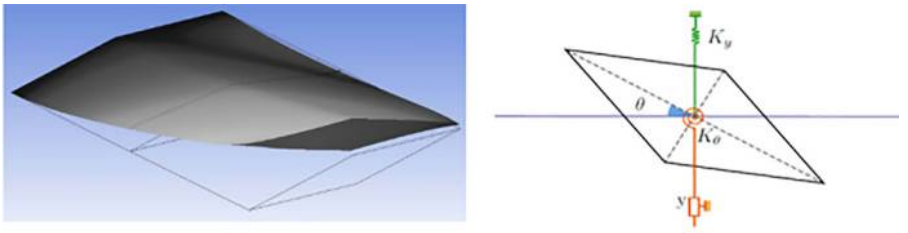

Figure 16.

The dynamic response of the aileron is driven by the fundamental equation of dynamics. The ideal solution is to simulate the solid displacement in a fully coupled way with the flow. However, the large difference between the characteristic times of the fluid and the solid makes this approach impracticable in the present case. The method relies thus on a separation between the numerical simulation of the flow and the resolution of the aileron dynamics. As a first step, only flapping is considered, that is driven by equation (2):

$$M\ddot{x} + D\dot{x} + Kx = \sum F_A \tag{2}$$

with M the matrix of mass, D the damping matrix, K the stiffness matrix and F_A the aerodynamic forces. To simplify the problem, an equivalent homogeneous material is considered, so matrices are reduced to a scalar.

This equation is time marched by means of a classical four steps Runge–Kutta scheme. At each time step, the aerodynamic forces are composed of two components: one related to the phenomenon of buffet and one due to the reaction of the aerodynamic force, induced by the profile displacement. The buffet force is extracted from the numerical simulations (URANS and LES database) and the aerodynamic response is modelled. Due to the low thickness of the profile, and the fact that displacement velocity is small compared to the fluid velocity, the lift force is modelled using the thin profile theory, with a compressibility correction (Anderson, 2007) [equation (3)]:

$$F_{lift} = \frac{2\pi(\alpha - \alpha_0)}{\sqrt{1 - Ma^2}} \times \frac{1}{2}\rho_\infty U_\infty^2 \cdot S \tag{3}$$

The angle of the flow seen by the profile at each instant of time is estimated as equation (4):

$$\tan\alpha = -\frac{\dot{x}}{U_\infty} \tag{4}$$

As the flow is responding in phase with the solid, the aerodynamic response is a positive damping term in the equation of the dynamic [equation (2)]. The main limitation of this approach is that the aerodynamic response to the profile displacement is instantaneous, while a lag is observed in practice. For this reason, this method is valid only when the ratio between the flow velocity and the displacement velocity of the solid is large (so the time lag becomes negligible). The results are expressed in terms of non-dimensional parameters U*, representing the ratio between the fluid velocity and the displacement velocity of the solid and m*, representing the mass ratio between the solid and the fluid:

$$U^* = \frac{U_\infty}{\frac{1}{2\pi}\sqrt{\frac{k}{m}} \cdot C} m^* = \frac{m}{\rho SL} \tag{5}$$

Table I.
Material properties of the aileron

	K	f [Hz]
Flexion	1373 N/m	13.2
Torsion	346 Nm	55.1

with k the stiffness, C the chord of the aileron and m the mass of the solid. In the case of the scaled 1:1 aileron, the value of the normalized velocity U* is estimated to be close to 100. Two cases are considered: without aerodynamic coupling (only the force coming from buffet is applied) and with coupling (aerodynamic response of the profile is added). The evolution of the normalized displacement, y* y/C, with respect to the normalized velocity U* is represented in Figure 17(a) (using URANS data) and in Figure 17(b) (using LES data), for a large mass ratio parameter m* 1600.

In Figure 17(a), the peak close to U* 10 corresponds to the resonance between the natural frequency of the solid and the aerodynamic excitation (buffet). In the case of LES, the buffet is associated to a more complex signal in terms of spectral content, so two resonance frequencies are shown in Figure 17(b). In the uncoupled case, the maximum displacement increased with U* (corresponding to a reduction of the stiffness). In the coupled case, as expected, the aerodynamic forces act as a damping term, which reduced the amplitude of the displacement, especially at the resonance frequency. A plateau is also reached for U* values higher than 500. At such velocity ratios, the periodic excitation due to buffet is no longer seen by the solid (as the time-average force of buffet is null, the solid does not react to this phenomenon). The effect of buffet predicted by LES has a weaker effect on the solid displacement compared to URANS.

Two normalized masses are compared: m* 80 (light hollow aileron) and m* 1600 (heavy plain aileron). The previous conclusions are globally unchanged with the lower mass ratio parameter (m* 80), as shown in Figure 18. However, as expected, the maximum displacement is increased (especially at low to moderate U* values) and a smoothening of the resonance peak, due to an increase of the aerodynamic damping (velocity displacement of the solid is increased compared to m* 1600, and so the value of the flow angle is also increased). In all cases, the value of the angle stays below 7-8 degrees, which is still acceptable for the thin profile theory.

5. Conclusion

Both experimental and numerical investigations have been performed to understand buffeting phenomenon and its impact on the composite aileron. This study can be summarized as follows. First, buffeting appears at transonic speed – for Mach numbers ranging from Ma 0.73 to Ma 0.81 – on a diamond aileron at 0° angle of attack, as verified by both numerical simulations and measurements. Second, experimental approach also

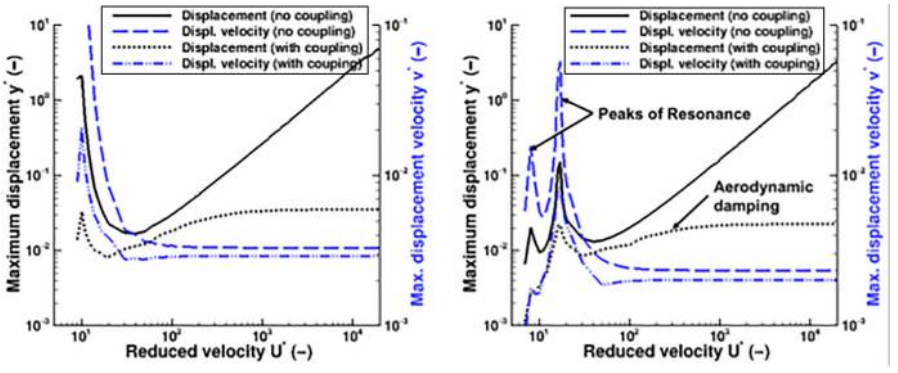

Figure 17.

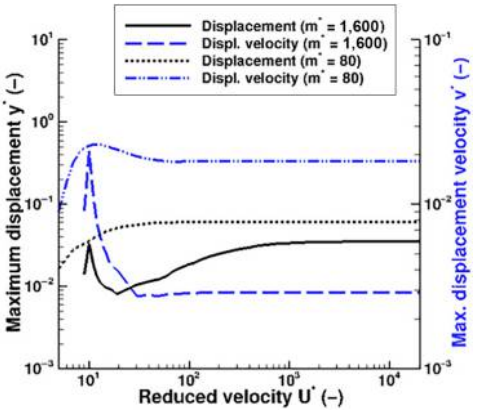

Figure 18.

reveals a 3D oscillation of the shock wave in the manner of a wind-flapping flag, but at this step, there is no clear evidence of the physical phenomena promoting this 3D mode. Third, LES identifies an oscillation of the width of the shock foot (λ -width) which has a significant impact on the aerodynamics load, but this phenomenon is not seen with the URANS simulations. At last, interestingly enough, the experiments have also highlighted the chaotic behavior of the shock wave as it shifts from an oscillatory periodic state (delta state) to an erratic 3D flapping state (flag state), transiently separated by transition states, where the shock wave moves from a close-to-trailing edge position (delta state) to a close-to-dihedron position (flag state).

This study allows the creation of a first experimental and numerical database of buffeting on diamond geometry which, to the authors' knowledge, has not been documented in the literature. Moreover, as mentioned by several authors as Sartor and Timme (2016), URANS confirms to be efficient to globally predict the buffet phenomenon, even if LES can improve the turbulence description.

However, the results reported in this paper still highlight a lack of deciphering of the buffeting origin. Exhaustive 3D numerical simulationsare to be conducted to better understand the spanwise oscillation of the shock wave, as observed in the wind tunnel experiments. To this avail more information are also required regarding the wind tunnel upstream flow conditions. The use of unsteady pressure sensors on the aileron will provide a more accurate validation of the numerical simulations in the future. Fluid/structure interaction has been investigated, considering only the bending mode. The effect of torsion should now be investigated since it should have more impact on the flow due to the increase of incidence that amplifies buffeting effects. A provision for future work will also consist in using a time-dependent stiffness, to represent the influence of progressive damages of unsteady loads on the aileron (fatigue).

References

Anderson, J. D. (2007), *Fundamental of Aerodynamics*, McGraw Hill.

Barakos, G. and Drikakis, D. (2000), "Numerical simulation of transonic buffet flows using various turbulence closures", *International Journal of Heat and Fluid Flow*, Vol. 21 No. 5, pp. 620 626.

Bermejo Moreno, I., Bodart, J., Larsson, J., Barney, B., Nichols, J.W. and Jones, S. (2014), "Solving the compressible Navier Stokes equations on up to 1.97 million cores and 4.1 trillion grid points", in

SC '13: Proceedings of the International Conference on High Performance Computing, Networking, Storage and Analysis in Denver, CO, USA, 2013, *IEEE*, pp. 1 10.

Berthelot, J. M. (2012), *Comportement Mécanique et Analyse des Structures. Materiaux Composites*, Editions TEC DOC, 5eme édition.

Brunet, V. (2003), "Computational study of buffet phenomenon with URANS equations", AIAA Paper, No. 2003 3679, Orlando, FL.

Brunet, V. and Deck, S. (2008), "Zonal detached eddy simulation of transonic buffet on a civil aircraft type configuration", in Peng, S. H. and Haase, W. (Eds), *Advances in Hybrid RANS LES Modelling*, Springer Berlin Heidelberg, pp. 182 191.

Burnham, J.K., Pitt, D.M., White, E.V., Henderson, D.A. and Moses, R.W. (2001), "An advanced buffet load alleviation system", in *42ndAIAA/ASME/ASCE/AHS/ASC Structures, Structural Dynamics, and Materials Conference and Exhibition in Seattle, WA, USA*, 16 19 April 2001.

Caruana, D., Mignosi, A., Correge, M., Le Pourhiet, A. and Rodde, A.M. (2005), "Buffet and buffeting control in transonic flow", *Aerospace Science and Technology*, Vol. 9 No. 7, pp. 605 616.

Corre, C., Renaud, T. and Lerat, A. (2003), "Transonic flow control using a Navier Stokes solver and a multi objective genetic algorithm", in *IUTAM Symposium Transsonicum IV*, pp. 297 302.

Crouch, J.D., Garbaruk, A., Magidov, D. and Travin, A. (2009), "Origin of transonic buffet on aerofoils", *Journal of Fluid Mechanics*, Vol. 628, pp. 357 369.

Gao, C., Zhang, W., Kou, J., Liu, Y. and Ye, Z. (2017), "Active control of transonic buffet flow", *Journal of Fluid Mechanics*, Vol. 824, pp. 312 351.

Goncalves, E. and Houdeville, R. (2004), "Turbulence model and numerical scheme assessment for buffet computations", *International Journal for Numerical Methods in Fluids*, Vol. 46 No. 11, pp. 1127 1152.

Iorio, M.C., Gonzalez, L.M. and Ferrer, E. (2014), "Direct and adjoint global stability analysis of turbulent transonic flows over a NACA0012 profile", *International Journal for Numerical Methods in Fluids*, Vol. 46 No. 11, pp. 1127 1152.

Iovnovich, M. and Raveh, D.E. (2012), "Reynolds averaged Navier Stokes study of the shock buffet instability mechanism", *AIAA Journal*, Vol. 50 No. 4, pp. 880 890.

Jacquin, L., Molton, P., Deck, S., Maury, B. and Soulevant, D. (2009), "Experimental study of shock oscillation over a transonic supercritical profile", *AIAA Journal*, Vol. 47 No. 9, pp. 1985 1994.

Kawai, S. and Larsson, J. (2012), "Wall modeling in large eddy simulation: length scales, grid resolution, and accuracy", *Physics of Fluids*, Vol. 24 No. 1, p. 015105.

Lee, B.H.K. (1990), "Oscillatory shock motion caused by transonic shock boundary layer interaction", *AIAA Journal*, Vol. 28 No. 5, pp. 942 944.

Lee, B.H.K. (2001), "Self sustained shock oscillations on airfoils at transonic speeds", *Progress in Aerospace Sciences*, Vol. 37 No. 2, pp. 147 196.

McDevitt, J.B. and Okuno, A.F. (1985), "Static and dynamic pressure measurements on a NACA 0012 airfoil in the ames high reynolds number facility", Technical Report, 2485, NASA.

McDevitt, J.B., Levy, J.L.L. and Deiwert, G.S. (1976), "Transonic flow about a thick circular arc airfoil", *AIAA Journal*, Vol. 14 No. 5, pp. 606 613.

Menter, F.R. (1994), "Two equation eddy viscosity turbulence models for engineering applications", *AIAA Journal*, Vol. 32 No. 8, pp. 1598 1605.

Pearcey, A.H. and Rao, K. (1968), "The interaction between local effect at the shock and rear separation a source of a significant scale effects in wind tunnel tests on airfoils and wings", Technical Report, AGARD.

Renaud, T., Corre, C. and Lerat, A. (2001), "Efficient numerical simulation of buffet for airfoils transonic regime", In *International Forum on Aeroelasticity and Structural Dynamics*, pp. 29 37.

Sartor, F. and Timme, S. (2016), "Mach number effects on buffeting flow on a half wing body configuration", *International Journal of Numerical Methods for Heat and Fluid Flow*, Vol. 26 No. 7, pp. 2066 2080.

Sartor, F., Mettot, C. and Sipp, D. (2015), "Stability, receptivity and sensitivity analyses of buffeting transonic flow over a profile", *AIAA Journal*, Vol. 53 No. 7, pp. 1980 1993.

Sugioka, Y., Numata, D., Asai, K., Koike, S., Nakakita, K. and Koga, S. (2015), "Unsteady PSP measurement of transonic buffet on a wing", AIAA Paper, No. 2015 0025, Kissimmee, FL.

Thiery, M. and Coustols, E. (2006), "Numerical prediction of shock induced oscillations over a 2d airfoil: influence of turbulence modelling and test section walls", *International Journal of Heat and Fluid Flow*, Vol. 27 No. 4, pp. 661 670.

Tijdeman, J. (1968), "Investigations of the transonic flow around oscillating airfoils", Technical Report, TR 77090U, NLR.

Vreman, A.W. (2004), "An eddy viscosity subgrid scale model for turbulent shear flow: algebraic theory and applications", *Physics of Fluids*, Vol. 16 No. 10, pp. 3670 3681.

Corresponding author
Jéromine Dumon can be contacted at: Jeromine.DUMON@isae.fr